Developmental Stage and Cellular Context Determine Oncogenic and Molecular Outcomes of *Ezh2*^{Y641F} Mutation in Hematopoiesis

Sarah M. Zimmerman[1,2,4], Samantha J. Procasky[,2,4], Sofia R. Smith[1,2,4], Jie-Yu Liu[5], Chad Torrice[5], George P. Souroullas[1,2,3,4, #]

[1] Department of Medicine,

[2] Division of Oncology, Molecular Oncology Section

[3] Siteman Comprehensive Cancer Center

[4] Washington University School of Medicine in St. Louis, St. Louis, Missouri, USA

[5] University of North Carolina, Chapel Hill, North Carolina, USA

[#]Address correspondence to G.P.S

George P. Souroullas, PhD

Washington University School of Medicine

Division of Oncology

Phone: (314) 362-8967

Abstract

Mutations in the histone methyltransferase EZH2, particularly the Y641 hotspot mutation, have been implicated in hematologic malignancies, yet the effect of timing and cellular context on their oncogenic potential has remained unknown. In this study, we utilized a conditional allele with tissue-specific Cre drivers to investigate the effects of *Ezh2*^{Y641F} mutations at various stages of development, with a focus on the hematopoietic system. We found that ubiquitous heterozygous *Ezh2*^{Y641F} expression at birth, or conditional expression in hematopoietic or mesenchymal stem cells, led to decreased survival due to hematopoietic defects and bone marrow failure, with no evidence of malignancy. In contrast, *Ezh2*^{Y641F} expression in committed B cells drives lymphoma formation, highlighting the lineage-specific oncogenic activity of the mutation. Transcriptomic analysis of B cell progenitors revealed key pathway alterations between Cre models such as altered IL2-Stat5 signaling pathway, differential expression of E2F targets, and altered GTPase pathway expression driven by upregulation of Guanylate Binding Proteins (GBPs) in Mx1-Cre *Ezh2*^{Y641F} pro-B cells. We further found that the GBP locus is regulated by Ezh2-mediated H3K27me3, it is associated with poorer survival in Acute Myeloid Leukemia patients and has variable effects on apoptosis in human lymphoma and leukemia cell lines. These findings suggest that the *Ezh2*^{Y641F} mutation may alter immune regulatory pathways, cell differentiation and apoptosis, with potential implications for disease progression. Our results highlight the critical role of mutation timing and cellular context in EZH2-driven hematopoietic disease, resulting in distinct downstream changes that shape the oncogenic impact of EZH2.

Introduction

Mutations in the EZH2 gene, an important regulator of chromatin structure and gene expression, play crucial roles in both normal development and malignancy. EZH2 is the enzymatic subunit of the Polycomb Repressive Complex 2 (PRC2) and mediates the methylation of lysine 27 on histone 3 (H3K27), contributing to chromatin compaction and transcriptional repression. Genetic alterations in *EZH2* vary across cancer types, with its role ranging from tumor suppressive to oncogenic. For example, *EZH2* deletions are often observed in T cell acute lymphoblastic leukemia or acute myeloid leukemia, where it typically functions as a tumor suppressor [1–5]. In contrast, EZH2 amplifications or overexpression are common in solid tumors, such as breast, lung, prostate, melanoma, and other solid tumors, where it functions in an oncogenic manner [6–10].

A frequent genetic alteration in *EZH2* across various cancers is a point mutation at tyrosine 641 (Y641 - or Y646 depending on isoform) within its catalytic SET domain. These mutations are primarily found in mature B cell neoplasms such as Follicular Lymphoma (FL) and Diffuse Large B cell Lymphoma (DLBCL), with a mutation rate around 15-20% [11,12]. Mouse models designed to study the effect and consequences of *Ezh2*^{Y641} mutations have shown that Ezh2 is required for Germinal Center (GC) formation by repressing cell cycle genes and genes critical for proliferation of centroblasts. Furthermore, expression of mutant *Ezh2*^{Y641} results in GC hyperplasia and can drive the development of B cell lymphoma [6,8,13–15]. At the molecular level, these mutations were originally characterized as loss-of-function mutations [11], however, subsequent biochemical studies revealed that they possessed gain-of-function properties, showing increased enzymatic activity when nucleosomes are mono- or di-methylated [16,17]. However, when nucleosomes are not methylated, the Y641F mutant demonstrated almost no enzymatic activity [16]. These findings suggested that *EZH2*^{Y641} mutations must exist in the presence of wild-type Ezh2 that mediates the initial methylation steps, consistent with the fact that all *EZH2*^{Y641} mutations identified to date in human patients are heterozygous[12]. The global consequences of *Ezh2*^{Y641F} mutations across the genome include increased levels of H3K27me3, although with altered patterns of distribution - increased deposition in some regions, decreased in others, and spreading of H3K27me3 past canonical boundaries [6,14,18]. These observations suggest that *EZH2*^{Y641F} mutations are not purely gain-of-function but likely neomorphic, and distinct from simple overexpression of *EZH2*^{WT}.

The initial studies on *Ezh2*^{Y641F} mutations were focused on mouse and human mature B cell lymphoma models or patient-derived cell lines, given the prevalence of *EZH2*^{Y641} mutations in B cell neoplasms. However, a small subset of these mutations also appears in B cell lymphoblastic leukemias, acute myeloid leukemia (AML), and several solid tumors including melanoma, bone, breast, head and neck, mesothelioma and endometrial cancers (**Fig. 1a, b**). The mutations type is not specific to any cancer type. While Ezh2 also plays a critical role in hematopoietic stem cell functions [19–21], it is surprising that these mutations are infrequent in non-B cell malignancies (**Fig. 1a, b**), implying that the cell of origin significantly impacts their oncogenic potential, or that these clones are outcompeted by other oncogenic drivers.

Mechanistically, *Ezh2*^{Y641} mutations have been associated with diverse pathways. In lymphoma models, *Ezh2*^{Y641F} mutations are linked to disrupted differentiation programs [8], Myc transcriptional signatures [6,22], interference with p53-mediated mTORC1 signaling [23], and cooperation with Bcl2 and Bcl6 [6,8,13]. In solid tumors, *Ezh2*^{Y641F} expression in melanocytes cooperates with oncogenic *Braf*^{V600E} mutations, accelerating tumor onset and altering anti-tumor immunity through IFN signaling modulation [6,24–26]. The downstream effects, therefore, of *Ezh2*^{Y641F} mutations vary significantly by cell type and developmental context. While much is known about these mechanisms in mature B cell lymphomas, the role of *Ezh2*^{Y641F} mutations in other hematopoietic malignancies or non-melanoma solid tumors is less understood.

Outside of cancer, somatic mutations in EZH2, including those in the SET domain, have been identified in patients with Weaver syndrome, who are characterized by accelerated skeletal maturation and overall overgrowth, intellectual disability and increased cancer susceptibility [27–30]. Mutations so far characterized in patients tend to be missense or truncating mutations, one of which was modeled in a mouse, which exhibited mild overgrowth phenotypes and decreased overall H3K27me3. It remains unclear mechanistically how somatic mutations in EZH2 cause overgrowth phenotypes.

To address the gaps mentioned above, we investigated the role of *Ezh2*^{Y641F} mutations during different stages of hematopoietic development, and in various solid tumor contexts. We utilized tissue- and cell type-specific Cre driver alleles to explore phenotypic and oncogenic outcomes, identify downstream pathways, and examine how the timing and cell of origin influence the mutations long-term effects on B cell differentiation and transformation.

Results

Heterozygous expression of *Ezh2*^{Y641F} during early embryonic development results in developmental and hematopoietic defects and decreases survival

To explore the oncogenic potential of *Ezh2*^{Y641F} in various cell types, we utilized a conditional *Ezh2*^{Y641F} allele [6] that remains wild-type until Cre-mediated recombination converts it to the mutant form (**Fig. 1c**). We crossed the *Ezh2*^{Y641F} allele to four distinct Cre drivers **(Fig. 1d)**: i) the ubiquitously expressed and tamoxifen-inducible Ubc-Cre^{ERT2} [31], ii) the Prx1-Cre [32], which is expressed during early limb bud development, iii) the Mx1-Cre, which is expressed in early hematopoietic stem and progenitor cells [33], and iv) the CD19-Cre [34], which targets early B cell progenitors in the bone marrow. Since germline deletion of Ezh2 in the mouse is lethal, and *Ezh2*^{Y641F} mutations are always heterozygous in patients, we maintained these animals in a heterozygous state and confirmed proper allele recombination in multiple tissues (**Fig. 1e**). Recombination in Ubc-Cre^{ERT2} mice was induced by tamoxifen injections two days after birth and in the Mx1-Cre by poly(I:C) at weaning age.

We monitored these animals for at least six months and carefully assessed phenotypic differences compared to *Ezh2*^{WT} controls. Overall, all mice expressing *Ezh2*^{Y641F} exhibited decreased survival. Notably, only the CD19-Cre crosses developed B cell lymphoma (**Supp. Fig. 1a**), consistent with our previous findings [6]. The Prx1-Cre crosses exhibited lower body weight and joint-related skeletal defects (**Supp. Fig. 1b**) as evident by abnormal animal posture and locomotion. Mice in the Ubc-Cre^{ERT2}, Prx1-Cre and Mx1-Cre groups exhibited very similar hematopoietic defects such as anemia, enlarged spleens and reduced peripheral B cell output (**Fig. 1f**, **Supp. Fig. 1b-f**). Interestingly, none of these crosses resulted in the development of B cell lymphoma, or other malignancies, but instead showed signs of bone marrow failure by six months of age. This bone marrow failure and decreased survival limited further observation of other potential malignancies requiring longer latency periods.

Given these outcomes, and due to the known association of *Ezh2*^{Y641} mutations with hematopoietic malignancies, we focused our detailed investigation on the two hematopoietic-specific Cre drivers, the B cell specific CD19-Cre and the hematopoietic stem and progenitor Cre, Mx1. We hypothesized that the cell of origin during hematopoiesis critically determines the oncogenic potential of the *Ezh2*^{Y641F} mutation.

Expression of *Ezh2*^{Y641F} at hematopoietic stem cell stage impairs B cell output in the blood and a partial block in B cell development in the bone marrow

The absence of overt malignancy in the Mx1-Cre *Ezh2*^{Y641F} mice was unexpected, prompting a more detailed analysis of hematopoiesis across multiple organs. We monitored mice over time for changes in hematopoietic development and for signs of disease by frequent blood analysis using flow cytometry. In young mice (4-10 weeks old), flow cytometric analysis of peripheral blood revealed no changes in lymphoid or myeloid populations. However, as the mice aged, they exhibited increased mortality compared to Mx1-Cre *Ezh2*^{WT} control animals starting at 16 weeks old, with a median survival of 329 days (**Fig. 1g**). Older mice (post four months), displayed clear defects in blood production, characterized by a marked decrease in white blood cell counts, primarily driven by a significant decrease in lymphocytes. Additionally, these mice were anemic with low red blood cell counts and low platelets (**Fig. 2a-b)**. Flow cytometric analysis of the peripheral blood revealed that the decrease in lymphocytes was driven primarily by a decrease in B cells (**Fig. 2c, e**). To determine if defects in B cell differentiation in the bone marrow contributed to this phenotype, we analyzed B cell progenitor populations in the bone marrow of young animals. This analysis revealed a partial block in B cell development at the transition from pre-pro B cells to pro B cells (**Fig. 2f-g**). These data suggest that the expression of mutant *Ezh2*^{Y641F} in hematopoietic stem and progenitor cells significantly disrupts B cell development in the bone marrow, resulting in reduced mature B cell output in the peripheral blood.

Expression of *Ezh2*^{Y641F} in HSCs results in skewed hematopoietic progenitor populations, high bone mass and bone marrow failure.

Given the established oncogenic role of *Ezh2*^{Y641F} mutations in lymphoma, we hypothesized that the observed phenotypes in Mx1-Cre *Ezh2*^{WT} mice might be driven by an underlying hematopoietic malignancy. To explore this hypothesis, we first analyzed hematopoietic progenitor populations in the bone marrow. In young mice (2-3 months old), we did not find any significant differences between Mx1-Cre *Ezh2*^{WT} and Mx1-Cre *Ezh2*^{Y641F} (data not shown). However, by six months of age, we found that mice expressing *Ezh2*^{Y641F} exhibited decreased bone marrow cellularity (**Fig. 3a**), accompanied by significant skewing of hematopoietic progenitors towards proportionally more common lymphoid progenitors at the expense of myeloid progenitors (**Fig. 3b-d**). Notably, the bones of *Ezh2*^{Y641F} mice were pale, consistent with anemia and decreased hematopoietic production (**Fig. 3e**). To further investigate the possibility of lymphoid blasts or changes to the bone marrow microenvironment, we performed immunohistochemistry on bones that had been fixed and decalcified. We did not find any evidence of blasts or hematopoietic

malignancy, but instead found that mice expressing *Ezh2*^{Y641F} had significantly decreased bone marrow cellularity and increased trabecular bone mass (**Fig. 3f**). Throughout the study, these mice did not develop any kind of bone malignancy.

Although Cre expression under the Mx-1 promoter is mostly restricted to hematopoietic populations, its expression has been detected in other tissues, such as osteoclasts, which are derived from myeloid precursors [35]. This raises the possibility that *Ezh2*^{Y641F} expression in osteoclasts may disrupt bone resorption, leading to increased bone mass. This altered bone structure could subsequently constrain the bone marrow microenvironment, contributing to bone marrow failure.

Expression of *Ezh2*^{Y641F} at the hematopoietic stem cell stage causes bone marrow failure leading to extramedullary hematopoiesis

The absence of malignant transformation in Mx1-Cre *Ezh2*^{Y641F} animals was unexpected, particularly given that *Ezh2*^{Y641F} expression persisted across all B cells, and CD19-Cre *Ezh2*^{Y641F} mice developed B cell neoplasia before the onset of bone marrow failure in Mx1-Cre mice.[6] One possible explanation is that early changes to the bone marrow microenvironment restrict B cell development and output, thus reducing the likelihood of acquiring secondary mutations necessary for B cell transformation.

To investigate this possibility, we performed bone marrow transplantation assays using hematopoietic stem and progenitor cells isolated from Mx1-Cre *Ezh2*^{Y641F} and Mx1-Cre control mice. These assays were performed using donor bone marrow from young animals (~8 weeks old), prior to any detectable defects in progenitors or cellularity as described above. Equal numbers of test donor (CD45.2) and competitor (CD45.1) bone marrow cells (500K) were transplanted into lethally irradiated recipient mice (CD45.1) (**Fig. 3g**). Four weeks after the transplants, we treated all animals with three injections of poly(I:C) at a dose of 13 mg/kg every other day and subsequently analyzed peripheral blood chimerism starting at two weeks after the last dose. Peripheral blood analysis by flow cytometry before Cre induction with poly(I:C) showed no significant differences in engraftment or differentiation. However, by 24 weeks post Cre induction, there was a marked decline in peripheral blood chimerism from *Ezh2*^{Y641F} donor-derived cells, indicating a loss of self-renewal capacity. Additionally, these donor-derived cells exhibited an impaired ability to generate myeloid cells (**Fig. 3h**). These results are consistent with the observed skewing of progenitor populations in 6-month-old and older Mx1-Cre *Ezh2*^{Y641F} mice,

which showed reduced myeloid progenitors compared to Mx1-Cre controls (**Fig. 3c**). This suggests a cell intrinsic defect in HSCs to differentiate towards the myeloid lineage. This cell intrinsic defect in HSC function may also contribute towards bone marrow failure. Long term monitoring of these animals did not reveal any evidence of disease or differences in overall survival.

Extramedullary hematopoiesis in the spleens of Mx1-Cre *Ezh2*^{Y641F} mice

One of the most prominent phenotypes of Mx1-Cre *Ezh2*^{Y641F} mice was splenomegaly (**Fig. 4a-b**). To determine whether this phenotype was associated with a splenic malignancy, we performed immunohistochemistry and flow cytometry analysis from harvested splenocytes. We found that spleens from Mx1-Cre *Ezh2*^{Y641F} mice had proportionally lower number of B cells and a substantial increase in Ter119+ erythrocytes (**Fig. 4d**). Immunohistochemistry further demonstrated ectopic hematopoietic features consistent with extramedullary hematopoiesis (**Fig. 4c**), which is proliferation of hematopoietic tissues outside of the bone marrow. Flow cytometry analysis also identified significant enrichment for hematopoietic progenitor populations in the spleens (**Fig. 4e**). Extramedullary hematopoiesis can typically occur in the presence of malignancy in the bone marrow, or in this case, bone marrow failure due to disruption of the bone microenvironment.

Transcriptomic and pathway differences in B cell progenitors isolated from Mx1-Cre and CD19-Cre *Ezh2*^{Y641F}

The findings above suggest that B cell progenitors in Mx1-Cre *Ezh2*^{Y641F} mice exhibit significant intrinsic differences compared to those from CD19-Cre mice, and that the timing of this mutation must be critical for its oncogenic activity. To better understand the differences in cell intrinsic properties of B cells isolated from the two different Cre lines, we performed global gene expression analysis by RNA-seq (**Fig. 5a**). Since we observed changes in B cell differentiation at progenitor stages with expression of *Ezh2*^{Y641F}, we assessed differences of pro-B and pre-pro-B cells from the two different Cre crosses. To minimize experimental variation, we bred the same *Ezh2*^{Y641F} (Cre negative) male with different females, CD19-Cre or Mx1-Cre at the same time in the same cage, with the females separated before giving birth. At 12 weeks old, all mice from the Mx1-Cre groups were treated with poly(I:C) to induce Cre expression. Four weeks after poly(I:C) treatment, and at around 16-18 weeks old, an age where neither genotype exhibits any hematopoietic phenotypes, we isolated pro B and pre pro B cells from the bone marrow using

FACS and processed them for RNA-sequencing. Ezh2 recombination was confirmed by PCR on spleen samples from all mice (**Supp. Fig. 2**)

Analysis of gene expression data revealed both shared and distinct gene expression patterns between pro and pre-pro-B cells from the two Cre lines. Principal component analysis distinguished pro vs pre-pro B cells (PC1) and separated *Ezh2*^{WT} from *Ezh2*^{Y641F} (PC3) (**Fig. 5b)**. The separation between *Ezh2*^{WT} and *Ezh2*^{Y641F} in PC3 was more pronounced in Mx1-Cre mice compared to CD19-Cre, consistent with greater changes in gene expression with the Mx1-Cre crosses. Furthermore, the overlap in differentially expressed genes ($p<0.04$, top 1000 genes) was only 10% between the two crosses in pro B cells (**Fig. 5c)**. Notably, expression of *Ezh2*^{Y641F} via Mx1-Cre resulted in significantly more differentially expressed genes compared to CD19-Cre (**Fig. 5d**). Despite the limited overlap at the differentially expressed gene level, gene set enrichment analysis (GSEA) revealed significant overlap in hallmark signatures between the two Cre lines expressing *Ezh2*^{Y641F}. Common signatures included enrichment for both type I and II interferon signaling, IL2-STAT5 signaling and TNF-alpha signaling (**Fig. 5e-f**). Overlapping signatures using KEGG analysis also included known EZH2 targets consistent with prior studies [36], as expected.

We also identified distinct gene expression signatures for each Cre line. For example, BMP2 targets were enriched in the Mx1Cre *Ezh2*^{Y641F} pro B cells, while HOXA9-MEIS targets were significantly enriched in the CD19-Cre *Ezh2*^{Y641F} pro B cells, as compared to their respective Cre-only controls (**Supp. Fig. 3**). Both pathways are directly involved in B cell differentiation and transformation and could contribute to the different phenotypes we observe with expression of mutant *Ezh2*^{Y641F} at different stages of B cell development.

Additionally, some hallmark signatures were enriched in opposite directions between the two Cre lines. These included the hallmark E2F-targets signature, which was enriched in the Mx1-Cre but depleted in the CD19-Cre (**Fig. 5e-f**), and heme metabolism, which was enriched in CD19-Cre but depleted in Mx1-Cre crosses (**Fig. 5e-f, Fig. 6b**). These signatures may underlie defects we observe in B cell development and differentiation, with E2F influencing cell cycle regulation, and heme metabolism via association with the Bach transcription factors [37] that control B cell differentiation.

Mx1-Cre *Ezh2*^{Y641F} transcriptomic changes are initiated during earlier developmental stages

In addition to pro B cells, we also analyzed gene expression changes in pre pro B cells in the Mx1-Cre crosses. Interestingly, we observed similar changes in pro and pre pro B cells from the Mx1-Cre *Ezh2*^{Y641F} compared to Mx1-Cre controls, such as enrichment for E2F targets, MYC targets, Interferon gamma response, in addition to depletion of heme metabolism (**Fig. 5f**). This suggests that the transcriptional differences driven by *Ezh2*^{Y641F} in pro B cells in the Mx1-Cre crosses start earlier and are maintained, again suggesting that the timing of mutations must be important for its downstream consequences.

Guanylate Binding Proteins (GBPs) are upregulated in Mx1-Cre *Ezh2*^{Y641F} pro B cells

Among the numerous genes differentially expressed in Mx1-Cre *Ezh2*^{Y641F} pro B cells, a cluster of GTPases, known as Guanylate Binding Proteins (GBPs), stood out due to their high expression level and significance. These GBPs - Gbp2, 3, 4, 7 and 8 – are located within the same chromosomal region, implying potential epigenetic co-regulation (**Fig. 6c-d**). The GBP genes were also part of the leading edge of several gene expression signatures characterized by GTPase activity (**Fig. 6a, e**). GBP genes are highly modulated interferon regulated genes that have mostly been studied for their role in immune response to infections [38,39]. In hematopoietic malignancies, previous studies have shown GBPs induce apoptosis in leukemia cells via interactions with MCL-1 and are associated with better prognosis [40]. In solid tumors, GBP activity has been linked to anti-tumor immunity, and some are used as prognostic biomarkers in solid tumors such as melanoma [41]. In hematopoietic cancers, GBP3, 4 and 7 combined tend to be overexpressed or amplified in 14% of AML patients (**Supp. Fig. 4a**). Their expression is also correlated with expression of major IFN regulators such as STAT1 and IRF1 (**Supp. Fig. 4b-c**).

GBP genes are clustered on human chromosome 1, and on chromosomes 3 and 5 in mice. Elevated GBP expression is common in many human cancers, with GBP1, 2, and 3 most highly expressed in cell lines from the ENCODE database (**Fig. 7a**). Additionally, expression of the GBP genes appears to be modulated on EZH2 activity. In human B cell lymphoma cell lines, EZH2 inhibition using GSK343 resulted in significant upregulation of several GBP genes, although there was also significant variability in expression (**Fig. 7b**). Analysis of ChIP-seq data from prior studies [22] showed increased H3K27me3 deposition across the entire *Gbp* locus in a mouse centroblasts and centrocytes expressing mutant *Ezh2*^{Y641F} compared to controls expressing wild-type Ezh2 (**Fig. 7c**). Additionally, EZH2 expression is negatively correlated with expression of

several *GBP* genes in DLBCL patients, (**Fig. 7d –** source: TCGA**)**. Combined, this data suggests that EZH2 likely controls expression of genes within this locus. While the role of *GBP* genes in hematopoietic malignancies remains underexplored, high GBP expression is associated with lower overall survival in AML patients (TCGA), with GBP2 showing particularly significant correlations (**Fig. 7e**). These data suggest that GBP levels could serve as biomarkers or influence disease progression and outcomes in hematologic malignancies.

To examine whether GBP overexpression impacts survival in different types of hematopoietic malignancies, we overexpressed human *GBP2*, one of the most highly upregulated *Gbp* genes in *Ezh2*^{Y641F} pro B cells, in two B cell progenitor (BCP) leukemia cell lines, five DLBCL lines and one AML cell line, and assayed rates of apoptosis (**Supp. Fig. 4d**). We found that overexpression of *GBP2* did not significantly affect apoptosis in AML or DLBCL lines. However, it resulted in a lower rate of apoptosis in the two pre-BCP leukemia cell lines, although not statistically significant, suggesting a potential lineage-specific function and effect (**Fig. 7f-g**). Various factors, such as the co-regulation of multiple GBP genes, might be necessary to elicit a more substantial impact on leukemia and cell growth. Moreover, the effect of specific GBP gene expression appears to be highly dependent on cellular context.

Discussion

In this study, we provide novel insights into the complex role of *EZH2*^{Y641F} mutations across various stages of hematopoietic development and different cancer types. By employing a conditional *Ezh2*^{Y641F} allele with tissue-specific Cre drivers, we have elucidated the mutation's diverse functional outcomes, offering a more nuanced understanding of its role in oncogenesis. These findings align with and extend the current literature, which predominantly focuses on the role of EZH2 mutations in B cell neoplasms. Our research reveals that the oncogenic potential of these mutations is significantly influenced by the timing of their occurrence and the specific cell type involved. This is particularly evident in the contrast between their effects in B cell lineage models, where they contribute to lymphoma development, and in other hematopoietic contexts, where they lead to different phenotypic outcomes.

The varied phenotypes we observe in this study underscore the profound impact of *Ezh2*^{Y641F} heterozygous expression on cellular processes. The decline in survival rates and the emergence of distinct phenotypes across different Cre crosses highlight both the tissue-specific and shared consequences of the mutation. For instance, the skeletal defects in Prx1-Cre crosses offer valuable insights into the mutation's diverse consequences across cell types and tissues, expanding our understanding of *Ezh2*^{Y641F} mutations beyond hematopoiesis. Hematopoietic defects such as bone marrow failure, extramedullary hematopoiesis, and blocks in B cell differentiation at the pre-B cell stage were consistently seen in Ubc-, Prx1-, and Mx1-Cre models. This points to a critical role for *Ezh2*^{Y641F} mutations in hematopoietic malignancies, where they are more commonly observed compared to solid tumors.

The absence of malignancy in Mx1-Cre *Ezh2*^{Y641F} mice underscores the developmental timing and cellular context in determining the oncogenic potential of *Ezh2*^{Y641F}. This aligns with previous reports of B cell lymphoma in CD19-Cre crosses, which points to lineage-specific susceptibility to transformation. Bone marrow failure was a consistent feature across all Cre crosses, except for CD19-Cre, suggesting a possible link between *Ezh2*^{Y641F} expression in bone progenitors and the high bone mass phenotype, especially noted in Ubc- and Prx1-Cre models. This phenotype could result from altered bone remodeling processes, potentially involving disrupted osteoclast function. *Ezh2*^{Y641F} expression in osteoclasts may interfere with normal bone resorption due to EZH2's role in silencing transcription factors that negatively regulate osteoclastogenesis [42–44].

While our studies showed that bone marrow failure is a consistent feature across all Cre crosses, except for CD19-Cre, bone marrow transplantation assays also revealed cell intrinsic defects in HSC self-renewal and myeloid differentiation in cells expressing mutant *Ezh2*^{Y641F}. This suggests that *Ezh2*^{Y641F} may affect cellular fitness, raising questions about the role of *Ezh2*^{Y641F} mutations in AML, where such mutations may not act as primary drivers, but potentially emerge as secondary mutations. This is supported by the low clonality (<5%) of Y641 mutations in AML, suggesting that they are not dominant oncogenic drivers and are likely outcompeted by other more potent oncogenic clones.

Transcriptomic analysis of B cell progenitors from Mx1-Cre and CD19-Cre *Ezh2*^{Y641F} models provided further evidence of the impact of developmental timing on the molecular outcomes of the mutation. The enrichment of pathways such as interferon signaling and cell cycle regulation highlights the complex role of *Ezh2*^{Y641F} in modulating immune responses and proliferation. A particularly notable discovery was the significant upregulation of *Gbp* genes in Mx1-Cre *Ezh2*^{Y641F} pro-B cells. GBPs, known for their role in immune responses, have also been implicated in apoptosis and anti-tumor immunity, yet their role in hematopoietic malignancies is less understood. The overexpression of *GBP* genes, particularly *GBP2*, in AML and B cell malignancies suggests potential involvement in disease progression and prognosis.

Our functional analysis revealed that overexpression of *GBP2* did not significantly impact apoptosis in AML or DLBCL cell lines but suggested lineage-specific effects in pre-BCP leukemia cell lines. These observations indicate that GBPs may act differently depending on cellular context and the co-expression of related genes, potentially offering new therapeutic targets or biomarkers for hematopoietic malignancies.

As with any study utilizing animal models, there are inherent limitations, including potential off-target effects of Cre recombination. The absence of malignancy in certain models may not negate the mutation's oncogenic potential in other tissues or under different conditions. Future studies should explore additional hematopoietic-specific Cre drivers, combinations with other oncogenic mutations, and longer monitoring periods to assess the full scope of the effects of *Ezh2*^{Y641F} mutations. Investigating chromatin and histone modifications post-*Ezh2*^{Y641F} expression could provide valuable insights into the mutation's impact on epigenetic landscapes and reveal mechanisms underlying its context-dependent behavior.

Our study sheds light on the complex interplay between mutation timing, tissue specificity, and hematopoietic outcomes associated with *Ezh2*^{Y641F} expression. The systemic impact observed, including B cell lymphoma and bone phenotypes, underscores the mutation's broad-reaching effects. The identification of *GBP* upregulation as a potential regulator of apoptosis in different hematopoietic lineages introduces new dimensions for future research into targeted therapies. While our findings advance the understanding of EZH2's role in hematopoietic development and disease, they also emphasize the importance of context in developing personalized cancer treatments. Continued exploration of *EZH2* mutations and their interactions with other oncogenic events will be crucial for refining therapeutic strategies and improving patient outcomes.

Materials and Methods

Mice

All mice were backcrossed to the C57Bl/6 background and housed in an Association for Assessment and Accreditation of Laboratory Animal Care (AAALAC)-accredited facility and treated in accordance with protocols approved by the Institutional Animal Care and Use Committee (IACUC) for animal research initially at the University of North Carolina-Chapel Hill, and later at Washington University in St. Louis. Both male and female mice were used in all experiments.

Genotyping

Genomic DNA was isolated from mouse tails and digested in DNA lysis buffer. Primer sequences for the Cre alleles were MB182F 5'-CAATGGTAGGCTCACTCTGGGAGATGATA-3', MB182R 5'-AACACACACTGGCAGGACTGGCTAGG-3', MB183F 5'-CAGGGTGTTATAAGCAATCCC-3', and MB183R 5'- CCTGGAAAATGCTTCTGTCCG-3'. Primer sequences for the *Ezh2*^{Y641F} allele were Forward 5'-CTCTTGGGGGTCAGTCCAC-3' and Reverse 5'-AAGTTGCTGAGTGTCTGGAAAA-3'.

Recombination of *Ezh2*^{Y641F} allele

The Mx-1-Cre allele is an inducible transgene. Expression of Mx-1-Cre was induced by intraperitoneal injection of polyinosinic-polycytidylic acid (polyI:C) (Sigma P0913 resuspended in PBS and filter sterilized), three injections every other day at 300 µg per dose. Expression of the Ubc-Cre^{ERT2} allele was induced by intraperitoneal injections of tamoxifen dissolved in corn oil at approximately 75 mg tamoxifen/kg body weight, at 2- and 4-days post birth. The CD19- and Prx1-Cre alleles are tissue-specific and not inducible. Recombination of the *Ezh2*^{Y641F} allele was determined by PCR on DNA isolated from mouse tissues, as indicated, using primers: Forward 5'- ACAGAAGTGAGAGAAGCTGATC-3' and Reverse 5'- GCTGCTACTATAAACAAGTC-3'.

Competitive bone marrow transplantation assays

Competitive bone marrow transplantation assays were performed by intravenous injections of a mixture of C57Bl/6 CD45.2 transgenic donor whole bone marrow and CD45.1 wild-type competitor bone marrow, 250K cells each. Both male and female mice were used as transplant recipients, all 8 weeks old. Transplant recipient mice were lethally irradiated with a split dose of 10.5 Gy, 5 hours apart.

Flow cytometry

For peripheral blood analysis, blood was collected using the cheek bleed method into tubes containing potassium EDTA. Complete blood counts were counted on a Hemavet (Drew Scientific). For flow cytometry analysis, red blood cells were lysed and samples stained with the appropriate cell surface markers as shown in Supp. Table X in HBSS buffer plus 2% FBS. Cells were analyzed in the same buffer plus 0.4 µg/ml propidium iodide. Various instruments were used for analysis, including LSRII (BD), Dako Cyan (Beckman Coulter) and Attune (Thermo). Hematopoietic progenitors were analyzed based on expression of cell surface markers that can be identified by flow cytometry as described (REF). Flow cytometry data were analyzed using FlowJo software (TreeStar Inc.). For the analysis of apoptotic cells, the cells were stained with Annexin-V-APC (Biolegend Cat# 640920) and 7-AAD Viability Staining Solution (Biolegend Cat# 420403).

Histology

Tissue was harvested and placed in 10% formalin overnight and then transferred to 70% ethanol until sectioning. Tissue was processed by Histowiz, embedded in paraffin, sectioned at 5 µm and stained with hematoxylin and eosin (H&E). For bone sectioning, femurs were collected, placed in 10% formalin overnight. Bones were decalcified using incubation with 10% EDTA pH7.2 for as long as two weeks at 4°C. Decalcified bones were then embedded into paraffin, sectioned and stained for H&E.

Bone marrow collection and FACS isolation of pro and pre-pro B cells

Bone marrow was collected from the femora and tibiae of CD19-Cre, CD19-Cre *Ezh2*^{Y641F}, Mx-1-Cre and Mx-1-Cre *Ezh2*^{Y641F} mice. The bones were flushed with HBSS and the bone marrow was homogenized by passing through a 18G needle and then strained through a 0.4 µm filter. Cells were washed once with HBSS and then stained with the following antibodies: CD19-APC (Biolegend 152409), CD43-FITC (Biolegend 143203), IgM-PE/Cy7 (Biolegend 406513), and B220-PB (Biolegend 103227) for 30 minutes on ice. Cells were washed and then resuspended in HBSS containing propidium iodide (Sigma P4864 at 1:500). Sorting was performed on propidium iodide negative cells to separate pro B cells (B220+, IgM+, CD19+, CD43+) and pre-pro B cells (B220+, IgM+, CD19-, CD43+) on the Sony iCyt Synergy BSC sorter at the Siteman Flow Cytometry Core.

RNA sequencing and analysis

RNA was prepared from FACS isolated pro and pre-pro B cells using the Qiagen RNeasy Micro kit (Qiagen 74004). Library preparation was handled by the GTAC core at Washington University. Specifically, samples were prepared according to library kit manufacturer's protocol, indexed, pooled, and sequenced on an Illumina NovaSeq 6000. Basecalls and demultiplexing were performed with Illumina's bcl2fastq2 software. RNA-seq reads were then aligned and quantitated to the Ensembl release 101 primary assembly. All gene counts were then imported into the R/Bioconductor package EdgeR1 and TMM normalization size factors were calculated to adjust for samples for differences in library size. Ribosomal genes and genes not expressed in the smallest group size minus one samples greater than one count-per-million were excluded from further analysis. The TMM size factors and the matrix of counts were then imported into the R/Bioconductor package Limma2. Weighted likelihoods based on the observed mean-variance relationship of every gene and sample were then calculated for all samples with the voomWithQualityWeights3 function and were fitted using a Limma generalized linear model with additional unknown latent effects as determined by surrogate variable analysis (SVA)4. The performance of all genes was assessed with plots of the residual standard deviation of every gene to their average log-count with a robustly fitted trend line of the residuals. Differential expression analysis was then performed to analyze for differences between conditions and the results were filtered for only those genes with Benjamini-Hochberg false-discovery rate adjusted p-values less than or equal to 0.05. For each contrast extracted with Limma, global perturbations in known Gene Ontology (GO) terms, MSigDb, and KEGG pathways were detected using the R/Bioconductor package GAGE5 to test for changes in expression of the reported log 2 fold-changes reported by Limma in each term versus the background log 2 fold-changes of all genes found outside the respective term. To find the most critical genes, the Limma voomWithQualityWeights transformed log 2 counts-per-million expression data was then analyzed via weighted gene correlation network analysis with the R/Bioconductor package WGCNA8. The RNA-seq data were uploaded to the Gene Expression Omnibus (GEO), accession number GSE270480.

Cell culture and generation of GBP2 overexpression cell lines

Cells were grown in RPMI medium 1640 (Gibco Cat# 11875-093) with 10% FBS (Millipore Sigma Cat# F0926) and 1% penicillin-streptomycin (Genesee Scientific Cat# 25-512). The GBP2 lentiviral vector (Vector Builder ID VB900000-0734xke) was used to overexpress human GBP2,

and the control vector is TLCV2 (Addgene 87360) with no sgRNA inserted. Cell lines include two B-ALL lines (TANOUE and REH), five DLBCL lines (WSU-NHL, RL, SUDHL6, Karpas-422, and HT), and one AML line (Kasumi-1). Lentivirus was produced in 293T cells via transfection with PEI, and then transduced into the cell lines listed above to generate GBP2 overexpression and control cell lines. These cells were selected for successful viral transduction using puromycin (Millipore Sigma Cat# P4512-1MLX10) at 3 µg/ml in the growth media, refreshed every other day for 7 days. Overexpression of *GBP2* was confirmed by qPCR.

RNA isolation and quantitative PCR

RNA was isolated from GBP2 overexpression and control cell lines using the PureLink™ RNA Mini Kit (Invitrogen Cat# 12183018A Lot# 2626710) according to the manufacturer's instructions. Synthesis of cDNA was performed using 1 µg RNA with the igScript™ First Strand cDNA Synthesis Kit (Intact Genomics Cat# 4314), and qPCR reactions were performed with the ig™ SYBR Green qPCR 2X Master Mix (Intact Genomics Cat# 3356 Lot# IH2902) on the BioRad CFX Connect Real-Time PCR Detection System. Primers for detecting human *GBP2* are Forward 5'-CAGTTGGAAGCAAGGCGAGAT-3' and Reverse 5'-GCACCTCTTTGGCCTGTATCC-3', and the primers for housekeeping gene *RPL27* are Forward 5'-ATCGCCAAGAGATCAAAGATAA-3' and Reverse 5'-TCTGAAGACATCCTTATTGACG-3'.

Statistical Analysis

Statistical analysis was performed using either GraphPad Prism software or Microsoft Excel. Bar graphs represent mean and either standard deviation or standard error of the mean as indicated in the figure legends. Sample sizes were determined based on pilot studies or historical data from similar experiments. Power analysis was performed for two-tailed analysis, under the assumption of normal distribution, with a significance level of 0.05 and power of 0.8. Differences between groups were determined using Student's t-test unless otherwise indicated in the figure legend.

Acknowledgements

We thank the Siteman Flow Cytometry Core and the McDonnell Genome Institute/Genome Technology Access Center at Washington University for flow cytometry services and genome analysis respectively, and the Department of Comparative Medicine for animal maintenance and expertise. We also thank all members of the Souroullas lab for insightful discussions and critical input on data analysis and presentation. This work was supported by the US National Cancer

Institute grants K22-CA229612-01 (GPS), T32 CA113275-10 (SZ), the Cancer Research Foundation, Chicago, IL (GPS), and the Leukemia Research Foundation (GPS).

Author contributions

SMZ, SJP, SRS, J-YL, CT and GPS performed experiments and analyzed data. J-YL performed experiments while at UNC-Chapel Hill and the work is not related to her current affiliation at Ochre Bio, Taipei, Taiwan. SMZ and GPS wrote the manuscript. GPS conceptualized and supervised the project.

Conflict-of-interest disclosure: The authors declare no competing financial interests.

Figure Legends

Figure 1. Expression of *Ezh2*^{Y641F} in hematopoietic stem cells shortens overall survival

a. Genetic alterations in EZH2 across mature B cell neoplasms, B cell leukemias (BLL), and acute myeloid leukemia (AML), analyzed using TCGA data from the Genie cohort (v16.1) on cBioPortal. B cell neoplasms, n=6444; BLL, n=911; AML, n=3859.

b. Frequency of *EZH2*^{Y641F} mutations across various cancer types, based on Genie cohort (v16.1) data analyzed via cBioPortal.

c. Schematic of Cre-lox strategy used to induce *Ezh2*^{Y641F} expression in mice.

d. Breeding strategy for cell type-specific expression of *Ezh2*^{Y641F} using different Cre drivers.

e. PCR confirmation of Ezh2 recombination in specific tissues by each Cre allele.

f. Summary of phenotypes observed in each Cre-driven *Ezh2*^{Y641F} expression model.

g. Disease-free survival curves for Mx1-Cre *Ezh2*^{Y641F} compared to Cre-only controls (log-rank test $p<0.0001$); median survival for Mx1-Cre *Ezh2*^{Y641F} mice is 329 days.

Figure 2. Partial block in B cell development in Mx1-Cre *Ezh2*^{Y641F} mice.

a. Complete peripheral blood cell counts (CBC) showing white blood cells (WBC), neutrophils (NE), lymphocytes (LY), red blood cells (RBC), and platelets in peripheral blood from Mx1-Cre *Ezh2*^{Y641F} and Mx1-Cre control mice, n>5 per group

b. Platelet counts from CBC analysis.

c. Flow cytometry analysis of peripheral blood in Mx1-Cre *Ezh2*^{Y641F} and Mx1-Cre only control mice, n>5.

d. Calculated absolute numbers of B cells, T cells and Myeloid cells in the peripheral of Mx1-Cre *Ezh2*^{Y641F} and Mx1-Cre control from flow cytometry (panel a) and CBC (panel c).

e. Representative flow plots of data in c.

f. Representative flow cytometry of bone marrow B cell progenitor populations in Mx1-Cre *Ezh2*^{Y641F} and Mx1-Cre only control mice; black box indicates pre-pro B cells.

g. Quantification of bone marrow B cell populations in Mx1-Cre *Ezh2*^{Y641F} and Mx1-Cre control mice, n>5. Error bars indicate standard deviation. * $p<0.01$, ** $p<0.001$.

Figure 3. Defective cell intrinsic hematopoietic stem cell function after induced expression of *Ezh2*^{Y641F}.

a. Total bone marrow cellularity in Mx1-Cre *Ezh2*^{Y641F} mice and Mx1-Cre control mice, n>5 per group.

b. Common Lymphoid Progenitors (CLP) counts in bone marrow of Mx1-Cre *Ezh2*^{Y641F} and Mx1-Cre only control mice, n>5.

c. Analysis of ckit+ Sca1+ Lineage negative (KSL) and multipotent progenitor (MP) populations.

d. Representative flow cytometry plots of bone marrow hematopoietic progenitor populations.

e. Image of tibiae from a Mx1-Cre *Ezh2*^{Y641F} mouse (right) and control (left).

f. H&E-stained bone sections from Mx1-Cre *Ezh2*^{Y641F} (bottom) and Mx1-Cre control mice (top).

g. Workflow for competitive bone marrow transplant assay with the indicated genotypes.

h. Donor cell engraftment analysis post competitive bone marrow transplant from, n=8 mice per group. Error bars represent standard deviation, * p<0.01, **p<0.001.

Figure 4. Extramedullary hematopoiesis in Mx1-Cre *Ezh2*^{Y641F} mice.

a. Spleen weight comparison in Mx1-Cre *Ezh2*^{Y641F} versus Mx1-Cre-only control mice, n>8-10 per group.

b. Representative images of spleen size (top) and cells in HBSS suspension (bottom).

c. H&E-stained spleen sections showing extramedullary hematopoiesis in Mx1-Cre *Ezh2*^{Y641F} and Mx1-Cre control mice.

d. Flow cytometry of blood lineage markers (B220, CD4, CD8, Mac1, Ter119) in spleen cells from Mx1-Cre *Ezh2*^{Y641F} and Mx1-Cre mice, n = 4-6.

e. Flow cytometry analysis of hematopoietic progenitor populations in spleens from Mx1-Cre *Ezh2*^{Y641F} and Mx1-Cre control mice; representative of three independent experiments.
Error bars represent standard deviation, * p<0.01, **p<0.001.

Figure 5. Global gene expression changes in pro and pre-pro B cells from CD19-Cre and Mx1-Cre driven expression of *Ezh2*^{Y641F}

a. Experimental schematic: RNA-seq was performed on pre-pro and pro B cells sorted from bone marrow of *Ezh2*^{WT} and *Ezh2*^{Y641F} from Mx1-Cre and CD19-Cre models.

b. Principal Component Analysis (PCA) plot of the RNA-seq data; pro B cells from Mx1-Cre *Ezh2*^{Y641F} and Mx1-Cre *Ezh2*^{WT} (control), n=3-4 per group.

c. Venn diagram showing overlap of the top differentially expressed genes (DEGs) in Mx1-Cre *Ezh2*^{Y641F} vs CD19-Cre *Ezh2*^{Y641F} pro B cells.

d. Volcano plots of DEGs in *Ezh2*^{Y641F} vs *Ezh2*^{WT} CD19-Cre pro B (left), *Ezh2*^{Y641F} vs *Ezh2*^{WT} Mx1-Cre pro B (center), and *Ezh2*^{Y641F} vs *Ezh2*^{WT} Mx1-Cre B pre pro B cells (right).
e-f. Gene set enrichment analysis (GSEA) of hallmark signatures in CD19-Cre (circles) and Mx1-Cre (triangles) *Ezh2*^{Y641F} pro- (e) and pre pro- (f) B cells.

Figure 6. Interferon, heme metabolism and GTPase activity gene expression signatures in *Ezh2*^{Y641F} pro B cells

a. Top: Heatmap of interferon gamma response signature enriched in Mx1-Cre *Ezh2*^{Y641F} compared to Mx1-Cre *Ezh2*^{WT} controls; bottom: enrichment curve and genes within the leading edge.
b. Top: Heatmap of heme metabolism signature, enriched in CD19-Cre *Ezh2*^{Y641F} and depleted in Mx1-Cre *Ezh2*^{Y641F}pro B cells; bottom: enrichment curves.
c. Top: Heatmap GTPase Activity genes, enriched in Mx1-Cre *Ezh2*^{Y641F} pro B cells compared to Mx1-Cre *Ezh2*^{WT} control; bottom: enrichment curve.
d. Volcano plot highlighting upregulated GBP genes in Mx1-Cre *Ezh2*^{Y641F} vs Mx1-Cre *Ezh2*^{WT} control pro B cells.
e. GSEA analysis of GTPase-related Gene Ontology (GO) terms in Mx1-Cre *Ezh2*^{Y641F} vs Mx1-Cre *Ezh2*^{WT} control pro B cells.

Figure 7. EZH2-mediated regulation of the GBP locus and its role in leukemia/lymphoma cell survival.

a. The human GBP gene cluster and transcript levels in ENCODE RNA-seq data various cell lines (K562, GM12878, H1-hESC, HeLa-S3, HepG2, HSMM, HUVEC, NHEK, NHLF).
b. GBP expression fold change post EZH2 inhibition with GSK343 in human lymphoma cell lines (data from GSE45982 [8,14]).
c. H3K27me3 ChIP-seq tracks in *Ezh2*^{WT} or *Ezh2*^{Y641F} mouse centroblasts and centrocytes at *Gbp* loci (data from GSE138036 [22]).
d. Correlation of *EZH2* and *GBP2* mRNA expression in AML patients (TCGA data analyzed via cBioPortal).
e. Overall survival in AML patients with altered *GBP* expression (all GBPs vs GBP2 specifically).

f. Flow cytometry analysis of apoptosis in GBP2 overexpressing vs and control cells (7-AAD and Annexin V staining). Results from two independent experiments.
g. Representative flow cytometry plots from (f). Error bars represent standard deviation.

Supplemental Figure Legends

Supplemental Figure 1. Ubc-CreERT2 and Prx1-Cre *Ezh2*^{Y641F} phenotypes.
a. Immunophenotyping of lymphoma cells from CD19-Cre *Ezh2*^{Y641F} mice, characterized by B220 low, IgM high, CD19+, CD43+ and CD5+.
b. Abnormal hind limb posture in Prx1-Cre *Ezh2*^{Y641F} mouse.
c. Comparison of body weight in Ubc-Cre^{ERT2} *Ezh2*^{Y641F} vs Ubc-Cre^{ERT2} control male and female mice.
d. Representative spleens showing splenomegaly in the Ubc-Cre^{ERT2} *Ezh2*^{Y641F} mice.
e. Flow cytometry analysis of spleen cells from Ubc-Cre^{ERT2} and Prx1-Cre lines with wild-type or mutant *Ezh2*^{Y641F} alleles.
f. Flow cytometry analysis of blood cells from Ubc-Cre^{ERT2} with wild-type or mutant *Ezh2*^{Y641F} alleles. Lineage markers used: B220 (B cells), Mac1 (myeloid cells), CD3 (T cells) and Ter119 (erythroid cells)

Supplemental Figure 2. Confirmation of *Ezh2*^{Y641F} recombination in B cell progenitor samples used for RNA sequencing
PCR analysis of Ezh2 recombination at the floxed locus, confirming conversion from wild-type *Ezh2* to mutant *Ezh2*^{Y641F}. PCR product at 410bp indicates the wild-type allele, while a 450bp product represents the recombined mutant allele. Positive control (Pos) is an *Ezh2*^{Y641F} melanoma cell line (Souroullas *et al.* 2016), and negative control (Neg) is a no-template control.

Supplemental Figure 3. Unique gene expression signatures in pro B cells
a. GSEA analysis shows enrichment of the Lee BMP2 Targets DN signature in Mx1-Cre *Ezh2*^{Y641F} pro B cells.

b. GSEA analysis shows enrichment of Hallmark MYC Targets V2 signature in Mx1-Cre *Ezh2*^{Y641F} pro B cells.

c. GSEA analysis shows enrichment of HOXA9 and MEIS1-regulated genes in CD19-Cre *Ezh2*^{Y641F} pro B cells.

Supplemental Figure 4. GBP gene expression in AML patients, expression correlations and GBP2 overexpression model

a. Frequency of GBP alterations in AML patients (TCGA data).

b. ReMap Atlas showing STAT1, STAT22, STAT3, STAT5 binding, and cis-regulatory elements at the GBP2 locus, as identified by ENCODE.

c. Correlation analyses of GBP1 with GBP4 (left), GBP4 with STAT1 (middle), and GBP2 with IRF1 (right) in DLBCL patients (TCGA DLBCL data, n=37, analyzed in cBioPortal).

d. Relative quantification of GBP2 expression by qPCR in the indicated human cell lines. Expression levels were normalized to RPL27, with fold changes calculated relative to cells transfected with an empty-vector control. Data represent the average of three replicate experiments; error bars indicate standard deviation.

References

1. Ntziachristos, P. *et al.* Genetic inactivation of the polycomb repressive complex 2 in T cell acute lymphoblastic leukemia. *Nature Medicine* **18**, 298–302 (2012).
2. Muto, T. *et al.* Concurrent loss of Ezh2and Tet2cooperates in the pathogenesis of myelodysplastic disorders. *J Exp Med* **210**, 2627–2639 (2013).
3. Clair, J. M.-S. *et al.* EZH2 couples pancreatic regeneration to neoplastic progression. *Genes & development* **26**, 439–444 (2012).
4. Wang, Y. *et al.* Ezh2 acts as a tumor suppressor in kras-driven lung adenocarcinoma. *International Journal of Biological Sciences* **13**, 652 (2017).
5. Mochizuki-Kashio, M. *et al.* Ezh2 loss in hematopoietic stem cells predisposes mice to develop heterogeneous malignancies in an Ezh1-dependent manner. *Blood* **126**, 1172–1183 (2015).
6. Souroullas, G. P. *et al.* An oncogenic Ezh2 mutation induces tumors through global redistribution of histone 3 lysine 27 trimethylation. *Nature Medicine* **22**, 632–640 (2016).
7. Zingg, D. *et al.* The epigenetic modifier EZH2 controls melanoma growth and metastasis through silencing of distinct tumour suppressors. *Nature Communications* **6**, 6051 (2015).
8. Béguelin, W. *et al.* EZH2 Is Required for Germinal Center Formation and Somatic EZH2 Mutations Promote Lymphoid Transformation. *Cancer Cell* **23**, 677–692 (2013).
9. Varambally, S. *et al.* The polycomb group protein EZH2 is involved in progression of prostate cancer. *Nature* **419**, 624–629 (2002).
10. Zhang, H. *et al.* Oncogenic Deregulation of EZH2 as an Opportunity for Targeted Therapy in Lung Cancer. *Cancer Discov* **6**, 1006–1021 (2016).
11. Morin, R. D. *et al.* Frequent mutation of histone-modifying genes in non-Hodgkin lymphoma. *Nature* **476**, 298–303 (2011).
12. Gao, J. *et al.* Integrative analysis of complex cancer genomics and clinical profiles using the cBioPortal. *Science Signaling* **6**, pl1–pl1 (2013).
13. Béguelin, W. *et al.* EZH2 and BCL6 Cooperate to Assemble CBX8-BCOR Complex to Repress Bivalent Promoters, Mediate Germinal Center Formation and Lymphomagenesis. *Cancer Cell* **30**, 197–213 (2016).
14. Béguelin, W. *et al.* EZH2 enables germinal centre formation through epigenetic silencing of CDKN1A and an Rb-E2F1 feedback loop. *Nat Commun* **8**, 877 (2017).
15. Caganova, M. *et al.* Germinal center dysregulation by histone methyltransferase EZH2 promotes lymphomagenesis. *J. Clin. Invest.* **123**, 5009–5022 (2013).

16. Sneeringer, C. J. *et al.* Coordinated activities of wild-type plus mutant EZH2 drive tumor-associated hypertrimethylation of lysine 27 on histone H3 (H3K27) in human B-cell lymphomas. *Proc. Natl. Acad. Sci. U.S.A.* **107**, 20980–20985 (2010).
17. Yap, D. B. *et al.* Somatic mutations at EZH2 Y641 act dominantly through a mechanism of selectively altered PRC2 catalytic activity, to increase H3K27 trimethylation. *Blood* **117**, 2451–2459 (2011).
18. Donaldson-Collier, M. C. *et al.* EZH2 oncogenic mutations drive epigenetic, transcriptional, and structural changes within chromatin domains. *Nature Publishing Group* 1–20 (2019) doi:10.1038/s41588-018-0338-y.
19. Xie, H. *et al.* Polycomb Repressive Complex 2 Regulates Normal Hematopoietic Stem Cell Function in a Developmental-Stage-Specific Manner. *Cell Stem Cell* **14**, 68–80 (2014).
20. Kamminga, L. M. *et al.* The Polycomb group gene Ezh2 prevents hematopoietic stem cell exhaustion. *Blood* **107**, 2170–2179 (2006).
21. Mochizuki-Kashio, M. *et al.* Dependency on the polycomb gene Ezh2 distinguishes fetal from adult hematopoietic stem cells. *Blood* **118**, 6553–6561 (2011).
22. Béguelin, W. *et al.* Mutant EZH2 Induces a Pre-malignant Lymphoma Niche by Reprogramming the Immune Response. *Cancer Cell* **37**, 655-673.e11 (2020).
23. Oricchio, E. *et al.* Genetic and epigenetic inactivation of SESTRIN1 controls mTORC1 and response to EZH2 inhibition in follicular lymphoma. *Science Translational Medicine* **9**, eaak9969 (2017).
24. Zingg, D. *et al.* The Histone Methyltransferase Ezh2 Controls Mechanisms of Adaptive Resistance to Tumor Immunotherapy. *CellReports* **20**, 854–867 (2017).
25. Zimmerman, S. M. *et al.* Ezh2Y641F mutations co-operate with Stat3 to regulate MHC class I antigen processing and alter the tumor immune response in melanoma. *Oncogene* (2022) doi:10.1038/s41388-022-02492-7.
26. Zimmerman, S. M., Suh, E., Smith, S. R. & Souroullas, G. P. Stat3-mediated Atg7 expression regulates anti-tumor immunity in mouse melanoma. *Cancer Immunol Immunother* **73**, 218 (2024).
27. Lui, J. C. *et al.* Ezh2 Mutations Found in the Weaver Overgrowth Syndrome Cause a Partial Loss of H3K27 Histone Methyltransferase Activity. *The Journal of Clinical Endocrinology & Metabolism* **103**, 1470–1478 (2017).
28. Tatton-Brown, K. *et al.* Weaver syndrome and EZH2mutations: Clarifying the clinical phenotype. *Am. J. Med. Genet.* **161**, 2972–2980 (2013).

29. Usemann, J., Ernst, T., Schäfer, V., Lehmberg, K. & Seeger, K. EZH2 mutation in an adolescent with Weaver syndrome developing acute myeloid leukemia and secondary hemophagocytic lymphohistiocytosis. *American Journal of Medical Genetics Part A* **170**, 1274–1277 (2016).
30. Basel-Vanagaite, L. Acute lymphoblastic leukemia in Weaver syndrome. *American Journal of Medical Genetics Part A* **152A**, 383–386 (2010).
31. Ruzankina, Y. *et al.* Deletion of the developmentally essential gene ATR in adult mice leads to age-related phenotypes and stem cell loss. *Cell Stem Cell* **1**, 113–126 (2007).
32. Logan, M. *et al.* Expression of Cre Recombinase in the developing mouse limb bud driven by a Prxl enhancer. *Genesis* **33**, 77–80 (2002).
33. Kühn, R., Schwenk, F., Aguet, M. & Rajewsky, K. Inducible gene targeting in mice. *Science* **269**, 1427–1429 (1995).
34. Rickert, R. C., Roes, J. & Rajewsky, K. B lymphocyte-specific, Cre-mediated mutagenesis in mice. *Nucl. Acids Res.* **25**, 1317–1318 (1997).
35. Aliprantis, A. O., Charles, J. F. & Nakamura, M. C. Chapter 2 - The Origins of the Osteoclast. in *Osteoimmunology (Second Edition)* (eds. Lorenzo, J., Horowitz, M. C., Choi, Y., Takayanagi, H. & Schett, G.) 5–23 (Academic Press, San Diego, 2016). doi:10.1016/B978-0-12-800571-2.00002-5.
36. Nuytten, M. *et al.* The transcriptional repressor NIPP1 is an essential player in EZH2-mediated gene silencing. *Oncogene* **27**, 1449–1460 (2008).
37. Watanabe-Matsui, M. *et al.* Heme regulates B-cell differentiation, antibody class switch, and heme oxygenase-1 expression in B cells as a ligand of Bach2. *Blood* **117**, 5438–5448 (2011).
38. Kim, B.-H. *et al.* A Family of IFN-γ–Inducible 65-kD GTPases Protects Against Bacterial Infection. *Science* **332**, 717–721 (2011).
39. Kirkby, M., Enosi Tuipulotu, D., Feng, S., Lo Pilato, J. & Man, S. M. Guanylate-binding proteins: mechanisms of pattern recognition and antimicrobial functions. *Trends in Biochemical Sciences* **48**, 883–893 (2023).
40. Luo, Y., Jin, H., Kim, J. H. & Bae, J. Guanylate-binding proteins induce apoptosis of leukemia cells by regulating MCL-1 and BAK. *Oncogenesis* **10**, 1–12 (2021).
41. Yingjuan, W., Li, Z., Wei, C. & Xiaoyuan, W. Identification of prognostic genes and construction of a novel gene signature in the skin melanoma based on the tumor microenvironment. *Medicine* **100**, e26017 (2021).

42. Fang, C. *et al.* Cutting Edge: EZH2 Promotes Osteoclastogenesis by Epigenetic Silencing of the Negative Regulator IRF8. *The Journal of Immunology* **196**, 4452–4456 (2016).
43. Adamik, J. *et al.* EZH2 Supports Osteoclast Differentiation and Bone Resorption Via Epigenetic and Cytoplasmic Targets. *Journal of Bone and Mineral Research* **35**, 181–195 (2020).
44. Caviness, P. C. *et al.* Decreased bone resorption in Ezh2 myeloid cell conditional knockout mouse model. *The FASEB Journal* **37**, e23019 (2023).

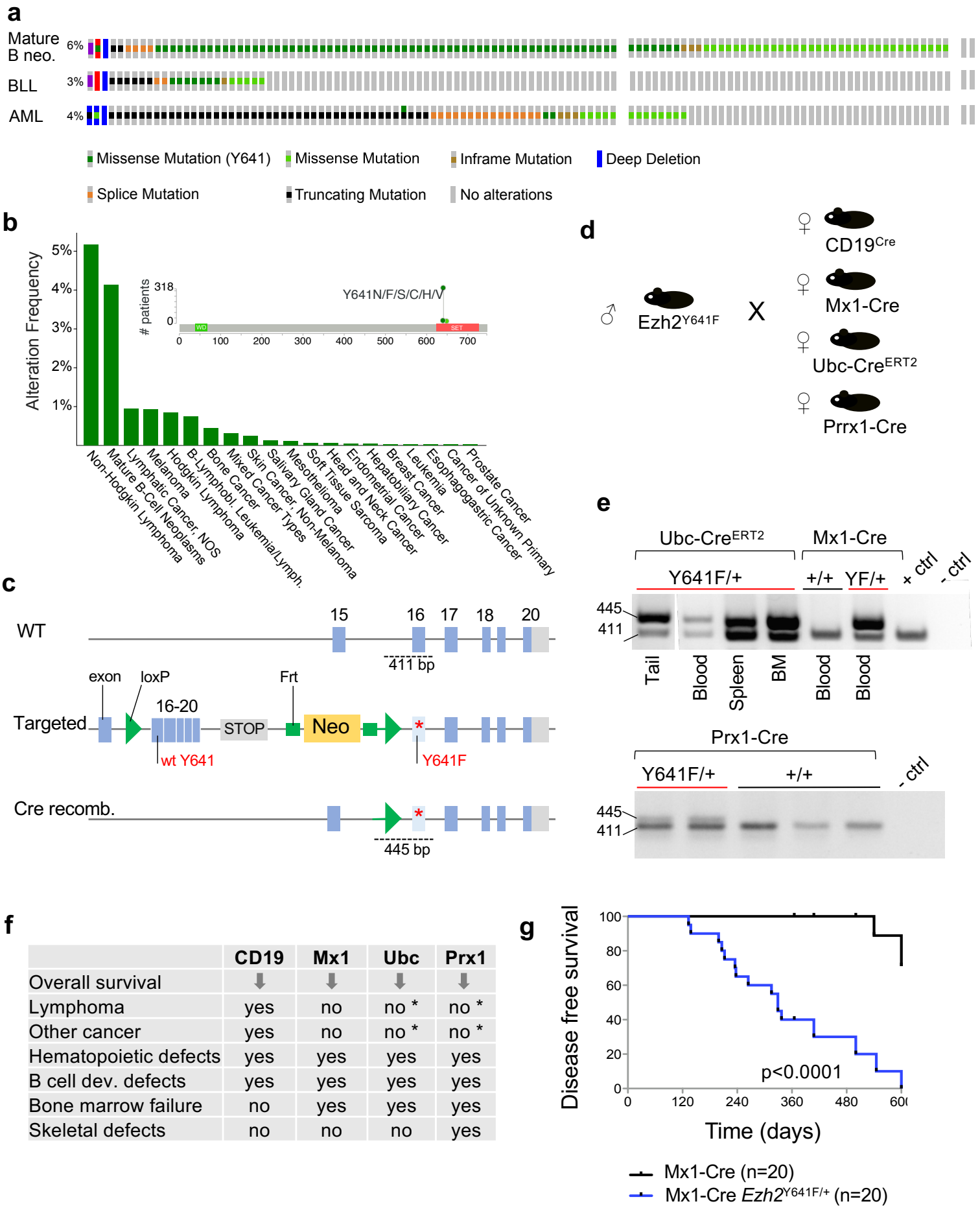

	CD19	Mx1	Ubc	Prx1
Overall survival	⬇	⬇	⬇	⬇
Lymphoma	yes	no	no *	no *
Other cancer	yes	no	no *	no *
Hematopoietic defects	yes	yes	yes	yes
B cell dev. defects	yes	yes	yes	yes
Bone marrow failure	no	yes	yes	yes
Skeletal defects	no	no	no	yes

Figure 1. Expression of *Ezh2*^{Y641F} in hematopoietic stem cells shortens overall survival

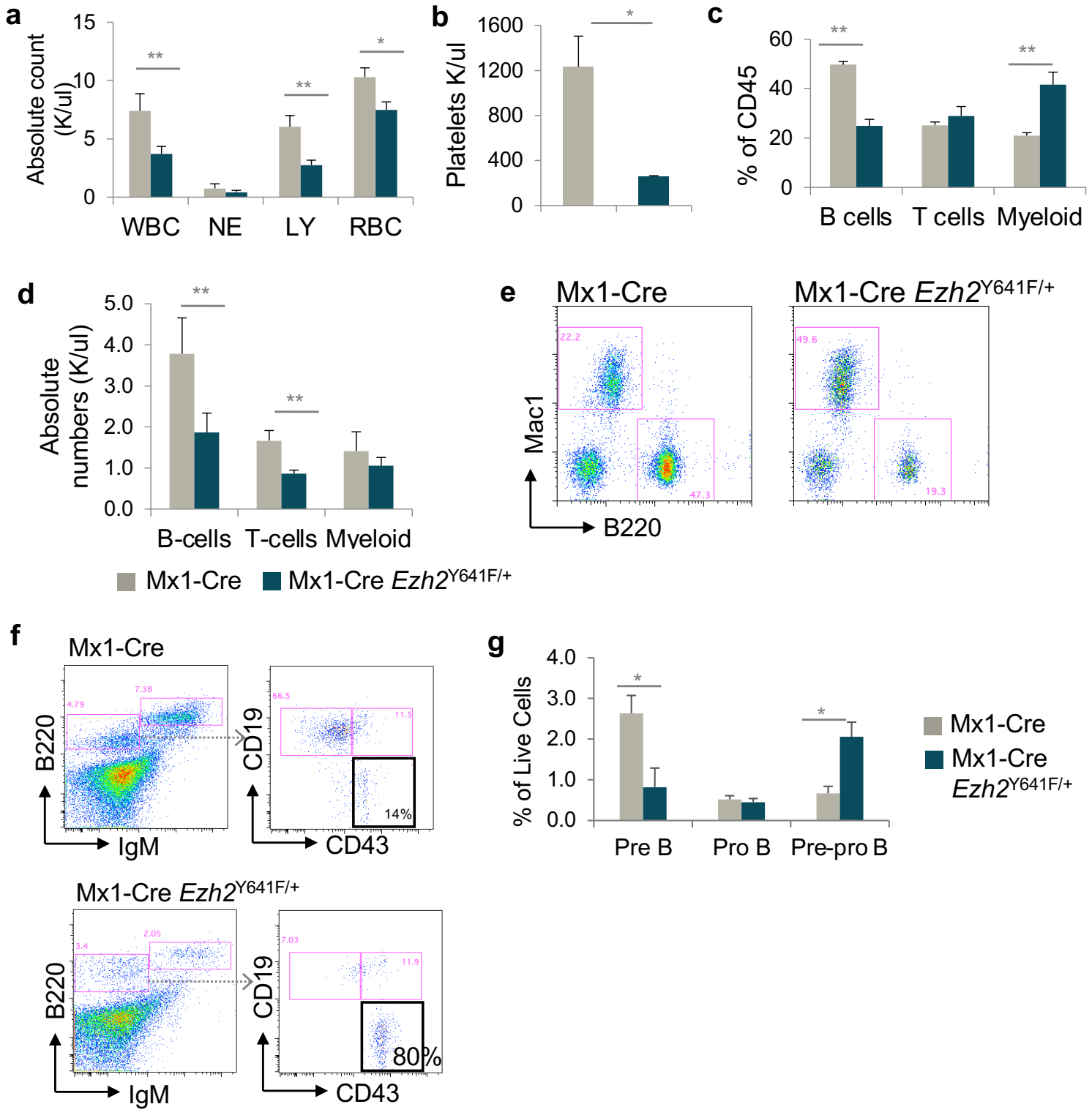

Figure 2. Partial block in B cell development in Mx1-Cre Ezh2$^{Y641F/+}$ mice

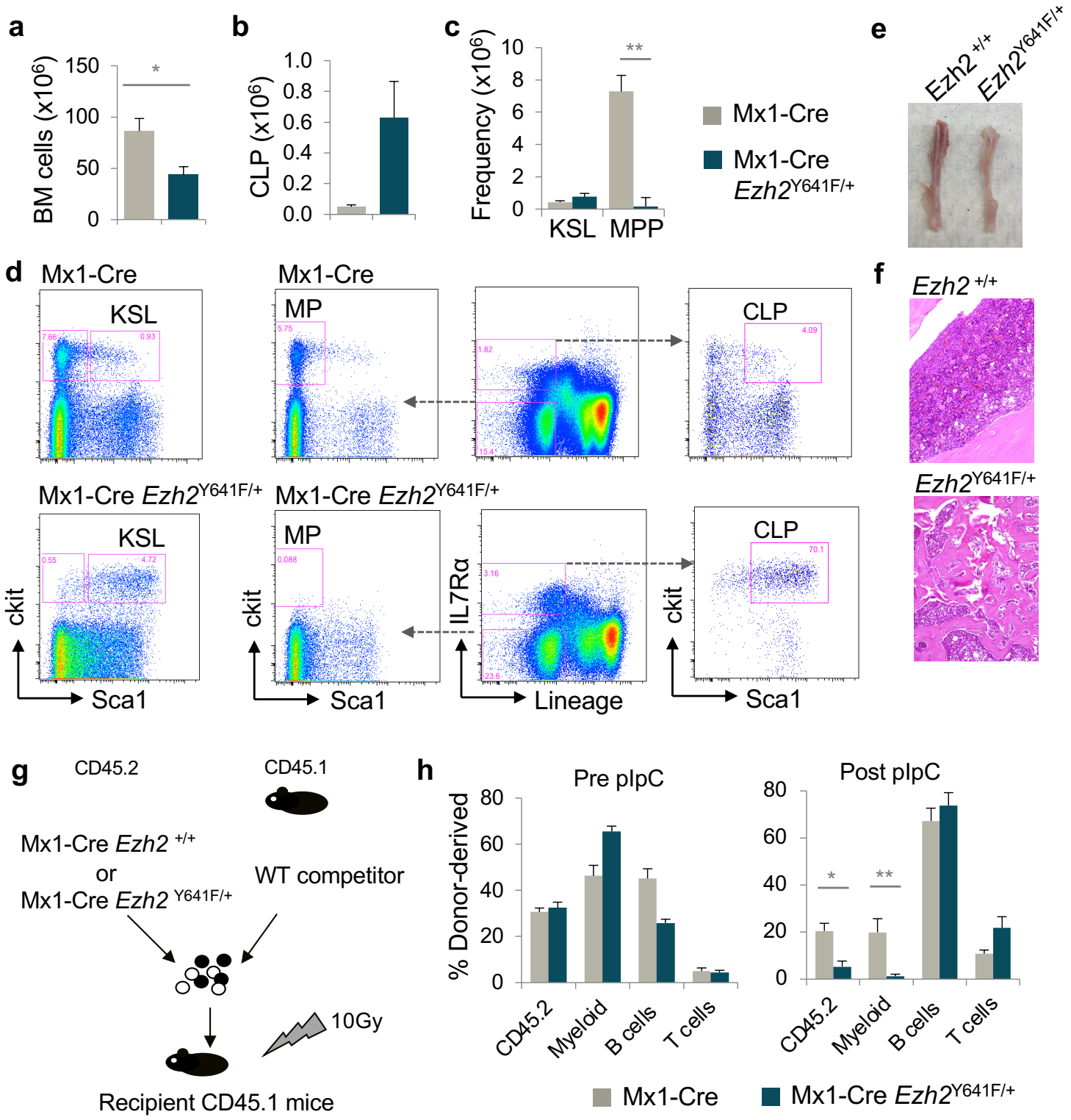

Figure 3. Defective cell intrinsic hematopoietic stem cell function after induced expression of *Ezh2*^{Y641F}

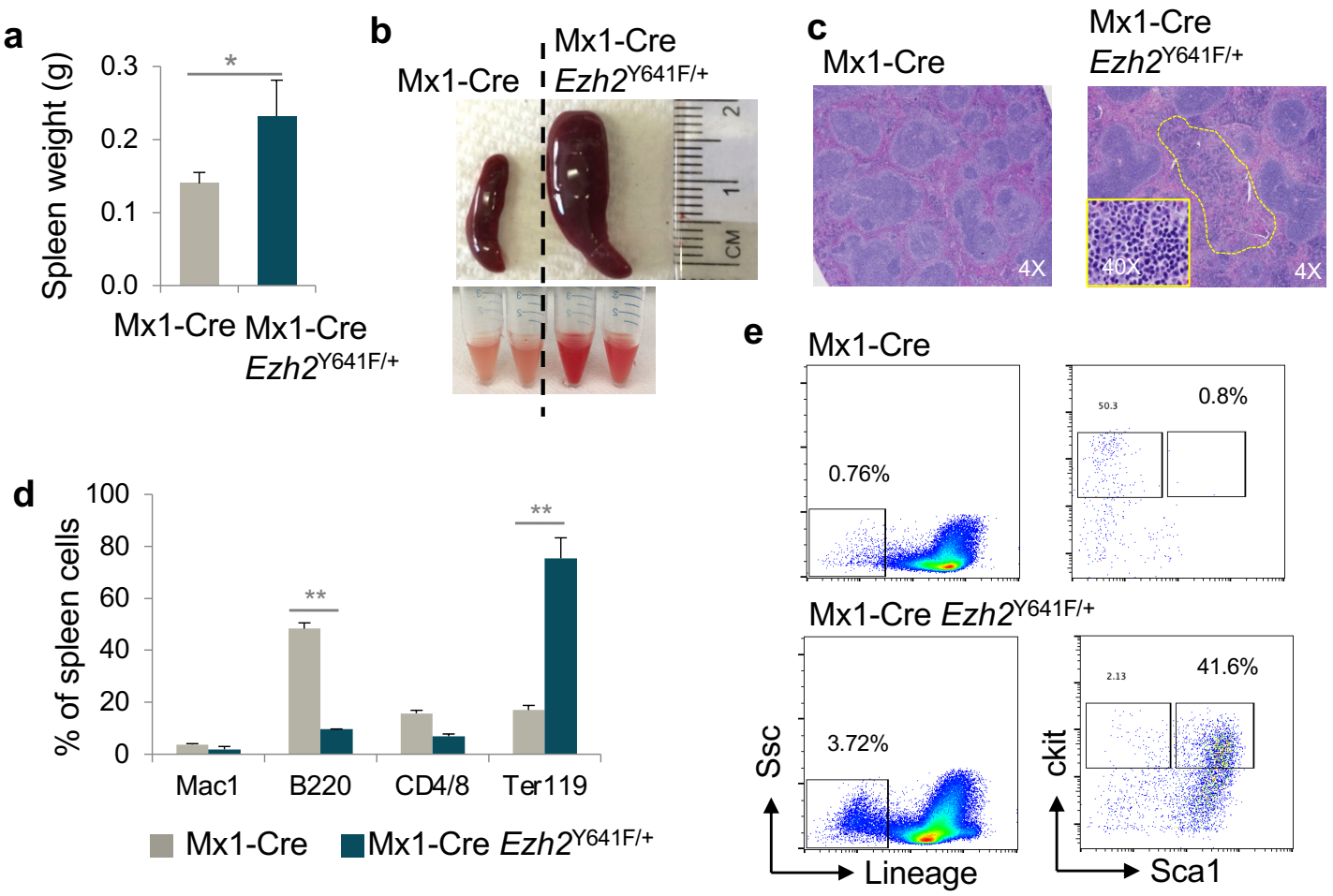

Figure 4. Extramedullary hematopoiesis in Mx1-Cre *Ezh2*^{Y641F} mice

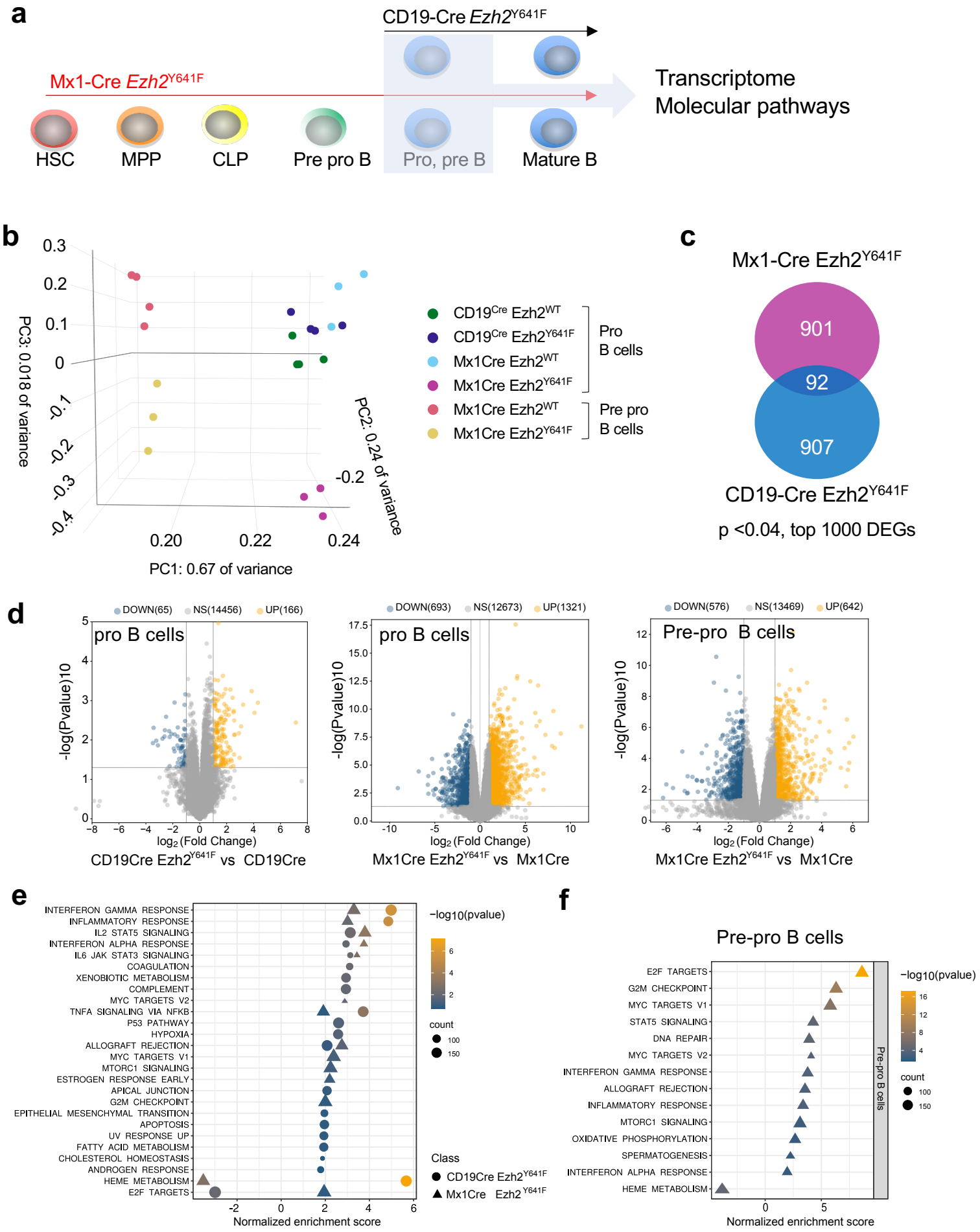

Figure 5. Global gene expression changes in pro and pre-pro B cells from CD19-Cre and Mx1-Cre driven expression of *Ezh2*^{Y641F}

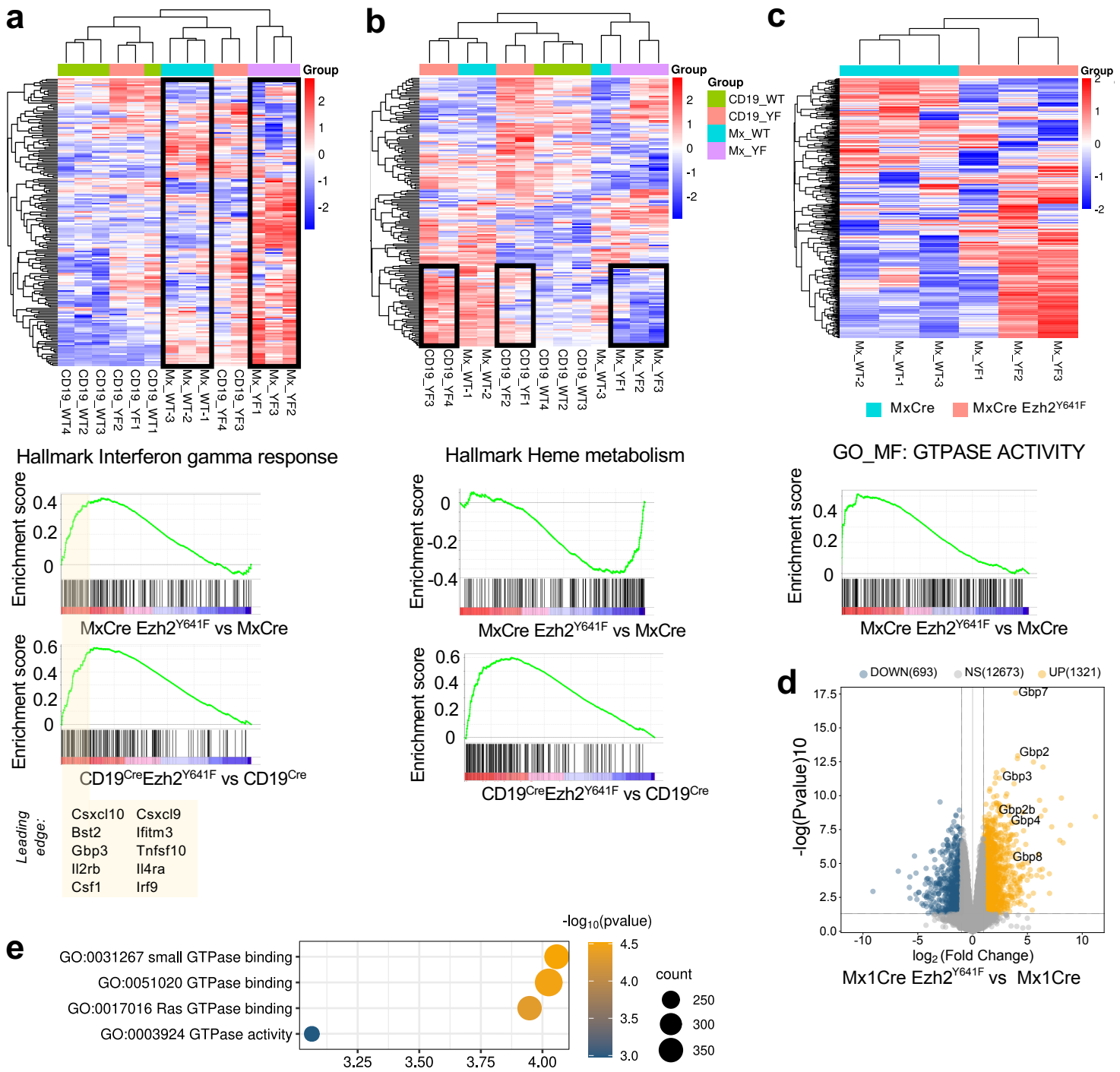

Figure 6. Interferon, heme metabolism and GTPase activity gene expression signatures in *Ezh2*^{Y641F} pro B cells

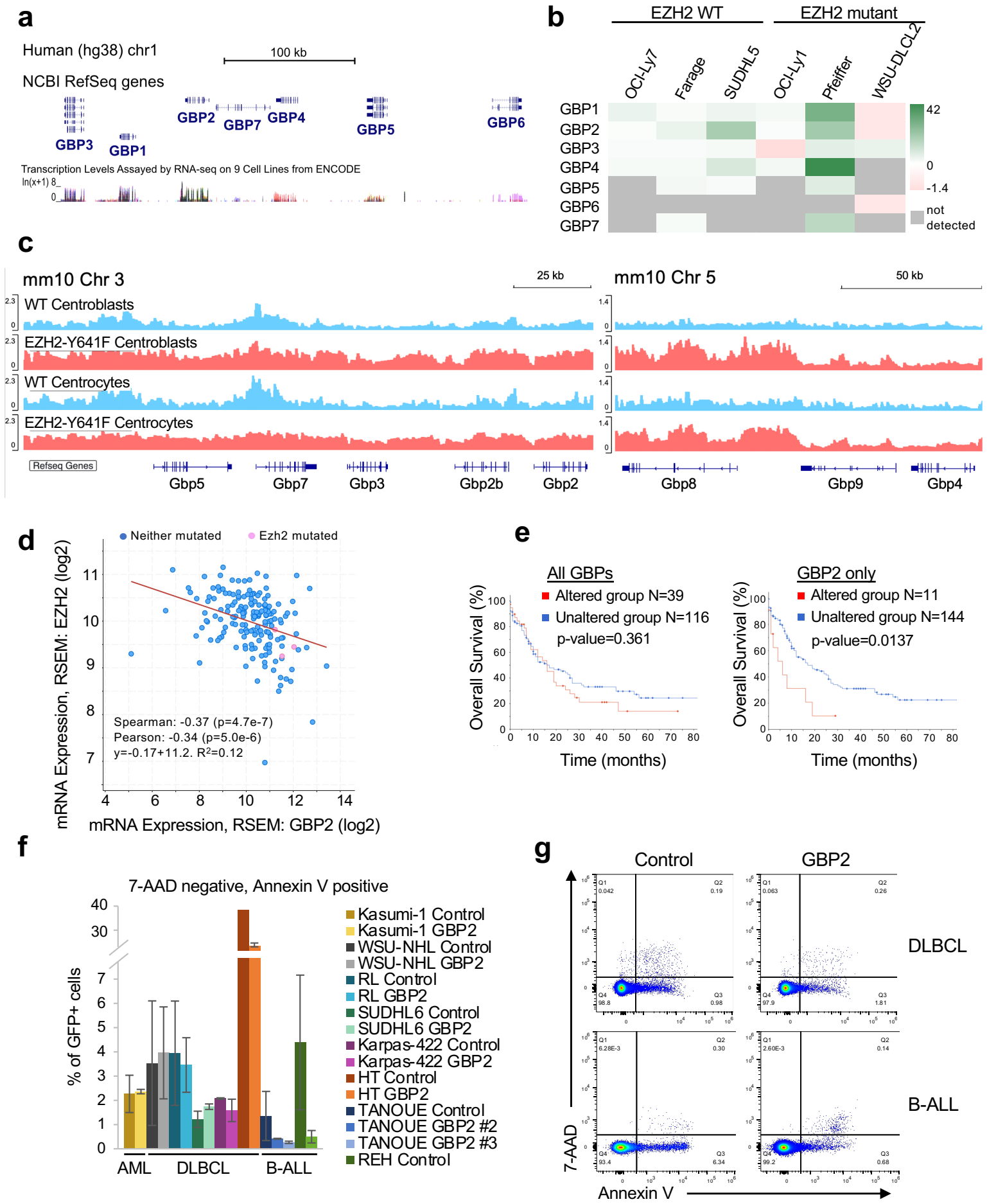

Figure 7. EZH2-mediated regulation of the GBP locus and its role in leukemia/ lymphoma cell survival.